AGU PUBLICATIONS

Earth's Future

RESEARCH ARTICLE
10.1002/2017EF000659

Model-Based Assessment of the CO_2 Sequestration Potential of Coastal Ocean Alkalinization

E. Y. Feng[1], W. Koeve[1], D. P. Keller[1], and A. Oschlies[1]

[1] Department of Biogeochemical Modelling, GEOMAR Helmholtz Centre for Ocean Research Kiel, Kiel, Germany

Key Points::
- For the first time coastal ocean alkalinization (COA) is tested in an Earth system model for its atmospheric CO_2 sequestration potential
- Olivine dissolution process is parameterized with olivine grain size, ambient water temperature and pH
- Ambitious COA will increase coastal $CaCO_3$ saturation and pH to very high levels well beyond the typical conditions

Supporting Information:
- Supporting Information S1

Correspondence to:
E. Y. Feng, yfeng@geomar.de

Citation:
Feng, E. Y., Koeve, W., Keller, D. P., & Oschlies, A. (2017). Model-Based Assessment of the CO_2 Sequestration Potential of Coastal Ocean Alkalinization, *Earth's Future*, *5*, 1252–1266, https://doi.org/10.1002/2017EF000659

Received 10 AUG 2017
Accepted 19 NOV 2017
Accepted article online 30 NOV 2017
Published online 22 DEC 2017

Abstract The potential of coastal ocean alkalinization (COA), a carbon dioxide removal (CDR) climate engineering strategy that chemically increases ocean carbon uptake and storage, is investigated with an Earth system model of intermediate complexity. The CDR potential and possible environmental side effects are estimated for various COA deployment scenarios, assuming olivine as the alkalinity source in ice-free coastal waters (about 8.6% of the global ocean's surface area), with dissolution rates being a function of grain size, ambient seawater temperature, and pH. Our results indicate that for a large-enough olivine deployment of small-enough grain sizes (10 μm), atmospheric CO_2 could be reduced by more than 800 GtC by the year 2100. However, COA with coarse olivine grains (1000 μm) has little CO_2 sequestration potential on this time scale. Ambitious CDR with fine olivine grains would increase coastal aragonite saturation Ω to levels well beyond those that are currently observed. When imposing upper limits for aragonite saturation levels (Ω_{lim}) in the grid boxes subject to COA ($\Omega_{lim} = 3.4$ and 9 chosen as examples), COA still has the potential to reduce atmospheric CO_2 by 265 GtC ($\Omega_{lim} = 3.4$) to 790 GtC ($\Omega_{lim} = 9$) and increase ocean carbon storage by 290 Gt ($\Omega_{lim} = 3.4$) to 913 Gt ($\Omega_{lim} = 9$) by year 2100.

1. Introduction

Anthropogenic emissions of the greenhouse gas CO_2 have led, and continue to lead, to elevated atmospheric CO_2 concentrations, causing global warming and associated environmental change with possibly severe consequences to the environment and society already over the next decades if emissions are not substantially reduced and eventually stopped (Intergovernmental Panel on Climate Change [IPCC], 2014). To reduce the risk of dangerous climate change, multiple adaptation and mitigation strategies are being implemented and even carbon dioxide removal (CDR) methods, which are nowadays also called "negative emission" technologies, are being discussed. Proposed CDR methods such as ocean iron fertilization or artificial upwelling appear to have relatively limited potential and considerable side effects (Keller et al., 2014), while methods such as direct air capture of CO_2 and bioenergy with carbon capture and storage (BECCS) require as yet undeveloped large capacities for storing CO_2 (National Research Council, 2015). The artificial increase of ocean alkalinity, artificial ocean alkalinization (AOA), is arguably the least represented negative emission technology in the literature (Bellamy et al., 2012), despite its high potential to reduce atmospheric CO_2 (González & Ilyina, 2016; Kheshgi, 1995) and mitigate ocean acidification (Feng et al., 2016; Taylor et al., 2015). Proposed AOA methods (see Renforth & Henderson, 2017 for a comprehensive review) include adding naturally abundant minerals, such as olivine ($(Mg^{2+},Fe^{2+})_2SiO_4$) (Köhler et al., 2010; Schuiling & Krijgsman, 2006) or limestone ($CaCO_3$) (Rau & Caldeira, 1999) directly to seawater. Olivine dissolution occurs naturally on timescales of thousands to millions of years during the process known as weathering (Kump et al., 2000). Hence, olivine-based AOA has also sometimes been referred to as "enhanced weathering" (Köhler et al., 2010). There have also been proposals to add anthropogenically produced minerals such as lime to seawater (either directly or after hydrolysis). More technical proposals include pumping seawater into reactors where it can react with carbonate or silicate minerals and CO_2 under controlled conditions or via electrolysis before the alkaline solution is added back to the ocean (House et al., 2007; Rau & Caldeira, 1999; Renforth et al., 2013). In all cases these methods will alter the carbonate chemistry of seawater and ultimately remove CO_2 from the atmosphere.

For AOA methods that involve adding olivine directly to seawater, a process that depends mainly on the mineral grain size, water temperature and pH, olivine reacts with CO_2 dissolved in seawater and

transforms it into bicarbonate and silicic acid (equation 1), thereby reducing sea surface CO_2 partial pressure and increasing CO_2 uptake from the atmosphere. In the new equilibrium with the atmosphere, the water with increased alkalinity has also increased dissolved inorganic carbon. The extra carbon is thought to be stored permanently in the ocean (Ilyina et al., 2013). At the same time, ocean acidification is mitigated, potentially protecting marine ecosystems, for example, tropical coral reefs (Albright et al., 2016; Feng et al., 2016). Previous studies have found that mineral particle size is one of the key factors determining the efficacy of olivine-based AOA as the time required for complete dissolution of olivine in seawater increases by approximately two orders of magnitude when olivine grain size increases from 10 to 1000 μm (Hangx & Spiers, 2009). With climate change elevated sea water temperature and ocean acidity could enhance olivine dissolution efficiency (Köhler et al., 2013). Limestone (calcium carbonate) can also react with dissolved CO_2 (equation 2). However, limestone can only dissolve within oceanic waters that are undersaturated with respect to $CaCO_3$ (Harvey, 2008; Millero, 2007). Such undersaturated waters are mostly found in the deep ocean, where the dissolution of any limestone will not stimulate oceanic CO_2 uptake from the atmosphere unless the water reaches the air-sea interface, for example, via upwelling. To overcome this dissolution barrier, some studies suggest reacting refined (ground) limestone with CO_2-rich gas streams in a water solution/spray, prior to adding the reaction products to the ocean (equation 2) (Rau, 2008; Rau et al., 2001). Alternatively, Renforth et al. (2013) suggest that lime (CaO) or quick lime ($Ca(OH)_2$), produced via calcination, could be added directly to the surface ocean where it would quickly dissolve and react with CO_2 (equation 3).

$$Mg_2SiO_4 + 4CO_2 + 4H_2O \rightarrow 2Mg^{2+} + 4HCO_3^- + H_4SiO_4 \quad (1)$$

$$CaCO_3 + CO_2 + H_2O \rightarrow Ca^{2+} + 2HCO_3^- \quad (2)$$

$$CaO + 2CO_2 + H_2O \rightarrow Ca^{2+} + 2HCO_3^- \quad (3)$$

Adding quick lime to the ocean has been simulated recently (Feng et al., 2016; Keller et al., 2014). Here, we focus on exploring the CDR potential and associated environmental impacts of olivine-based AOA (equation 1). An objective comparison of both methods, olivine-based versus lime-based AOA (or COA), is beyond these objectives, in particular, since it requires a solid socioeconomic analysis of mining capacities, energy investments and solutions to the CO_2-storage issue of lime-based technologies. Recent theoretical and modeling studies of olivine-based AOA in the open ocean (Köhler et al., 2013) and on coastal beaches (Hangx & Spiers, 2009) have suggested that the CDR potential of olivine-based AOA varies considerably with the specific implementation strategies. Concerning open ocean implementations, unless ground into sufficiently small particles, olivine grains will likely sink out of the surface mixed layer prior to completed dissolution (Köhler et al., 2013) and, hence, not efficiently increase ocean carbon uptake and storage. Since grinding is energy (and cost) intensive, grinding olivine would decrease the net efficiency in terms of CO_2 sequestration (Hangx & Spiers, 2009; Köhler et al., 2013).

Additionally, transport requirements for distributing olivine in the open ocean would further increase energy consumption and likely CO_2 emissions. Concerning AOA on coastal beaches (Schuiling & Krijgsman, 2006), transport and grinding requirements are expected to be considerably smaller. However, previous studies (Pokrovsky & Schott, 2000; Wogelius & Walther, 1991) have shown that the olivine dissolution rate will decline as ambient pH increases. Accordingly, the potential for dissolving olivine on relatively small beach areas may be limited because of the local pH elevation induced by olivine dissolution itself (Hartmann et al., 2013).

Given these likely limitations on implementing AOA in the open ocean and on coastal beaches, we consider the climate mitigation potential and environmental side effects of implementing AOA in "coastal seas" (Meysman & Montserrat, 2017; Montserrat et al., 2017), which includes oceanic continental shelves shallower than approximately 200 m; referred to hereafter as coastal ocean alkalinization (COA). For conceptual simplicity, we consider these coastal waters well mixed from the surface to seabed on at least an annual basis, driven, for example, by tidally and wind-induced turbulence and seasonally cycling surface buoyancy fluxes. Thus, we assume that even if olivine sinks to, and dissolves on, the coastal seabed, the water

with carbon chemistry altered by dissolution would be eventually mixed to the sea surface where it can take up additional CO_2 from the atmosphere. COA may therefore have a higher potential for olivine to increase ocean carbon uptake and storage than AOA in the open ocean, where olivine grains may sink out of the region in immediate or at least occasional contact with the atmosphere. Compared to olivine deployment on coastal beaches, the larger volume and rigorous mixing in coastal waters may also prevent pH from becoming too elevated locally. Moreover, coastal sea deployments would not depend on limited beach areas and could also be done in regions with rocky shorelines. While not taken into account in our assessment here, we also note that because of shorter transport distances, COA deployment logistics would probably be less costly and energy intensive than open ocean AOA (Hangx & Spiers, 2009; Köhler et al., 2013). As a side benefit, COA for CDR purposes may simultaneously be regarded as a strategy to mitigate regional coastal acidification (e.g., Feng et al., 2016).

Excessive alkalinity additions may perturb ocean biogeochemistry and cause undesirable side effects, for example, respiratory alkalosis and hyperkalemia of crustaceans (Cripps et al., 2013). There is also no well-established "upper limit" for $CaCO_3$ saturation, after which spontaneous, abiotic calcium carbonate or phosphate precipitation may occur (De Rooij et al., 1984; Marion et al., 2009) that can be used to guide olivine implementation. In ocean biogeochemistry, aragonite saturation Ω is widely adopted as a metric to characterize the saturation state of seawater with respect to aragonite ($CaCO_3$) mineral (Pilson, 2013). It is an open question to what extent additional constraints on Ω would reduce the potential of AOA or COA in particular.

In this study, we conduct several numerical experiments using an Earth system model of intermediate complexity to investigate the effectiveness of COA by simulating the global scale addition of olivine to coastal waters for a range of olivine grain sizes with an explicit parameterization of the temperature and pH dependence of the olivine dissolution process. First, we investigate the implications of adding massive amounts of olivine in a previously proposed 1:1 M ratio of alkalinity added to anthropogenic CO_2 emissions (Ilyina et al., 2013) in a business as usual scenario over the 21st century. Then, with a focus on understanding the CO_2 sequestration potential, while minimizing biogeochemical side effects, we examine upper-limit constraints on aragonite saturation levels, Ω, in the coastal deployment sites. Scales considered in this initial assessment cover hundreds of kilometers to the global ocean during the 21st century, with the aim to provide information about the possible overall potential of the idea of COA.

2. Materials and Methods

2.1. Model Description

Simulations are conducted with the University of Victoria Earth System Climate Model (version 2.9) (Eby et al., 2013; Weaver et al., 2001), which is an Earth system model of intermediate complexity. The model components include a three-dimensional general circulation model of the ocean (Pacanowski, 1996) that includes biogeochemistry (Keller et al., 2012), a terrestrial model (Meissner et al., 2003), a simple one-layer atmospheric energy-moisture balance model based on Fanning and Weaver (1996) and a dynamic-thermodynamic sea-ice model (Bitz & Liscomb, 1999). All components have a common horizontal resolution of 3.6° longitude × 1.8° latitude. The oceanic component has 19 vertical levels with thicknesses ranging from 50 m near the surface to 500 m in the deep ocean. Formulations of the air-sea gas exchange and seawater carbonate chemistry are based on the OCMIP (Ocean Carbon Cycle Model Intercomparison Project) abiotic protocol (Orr et al., 1999). Simulated sea surface temperature (SST) and oceanic pCO_2 have been evaluated against World Ocean Atlas (WOA; Locarnini et al., 2013) and Surface Ocean CO_2 Atlas (SOCAT; Landschützer et al., 2014) data (see Supporting materials of Feng et al., 2016). The evaluation showed that UVic can simulate sea surface pCO_2 within the range of observations, but that UVic also generates a slightly cooler Atlantic and warmer eastern continental boundaries, which is a common bias also in CMIP5 (Coupled Model Intercomparison Project) models (Wang et al., 2014).

2.2. COA Simulation Design

Simulated COA is implemented in all ocean grid cells that are adjacent to land between 58.5°N and 59.4°S (to exclude most ice-covered regions; Figure S1 in Supporting Information S1). The total surface area of these boxes amounts to 3.11×107 km^2, that is, 8.6% of the global ocean surface area. Collectively, we refer to these model grid cells as "coastal sea" regions in this study. These coastal seas are roughly consistent with

the national exclusive economic zones (EEZ), that is, waters extending seaward to a distance of 200 nautical miles (approximately 370 km) from the coastline. In our implementation of COA, for simplicity we assume that the waters in these coastal areas are well mixed. This ignores the fact that deep trenches or narrow continental shelves characterize some coastal regions, for example, in the eastern Pacific. We further assume that all undissolved olivine grains stay in the coastal deployment grid box, that is, they are not transported out of the region by currents, and are not buried in the sediments. In this study we also do not consider the unintentional addition of nutrients, such as Si or Fe, or other contaminants that may be contained in olivine rocks (Hauck et al., 2016; Köhler et al., 2013).

Olivine dissolution in aqueous environments is complex and an analytical function to describe how olivine dissolves in coastal seawater is not available. When olivine is added to coastal waters, potential pore water saturation in the seabed and secondary reactions will likely occur (Montserrat et al., 2017). In addition, the alternating layers (Mg-poor layers, SiO_4-coatings) generated on the olivine mineral surface can lead to non-stoichiometric dissolution (the number of dissolved atoms cannot be expressed as a ratio presented in the chemical formula) and temporal variations of the area-normalized olivine dissolution rates (Maher et al., 2016). Since a detailed understanding of these processes under typical seawater conditions is currently lacking, these complex interactions are ignored in our study. Instead, in this paper, the olivine dissolution process is described using a shrinking-core model (Hangx & Spiers, 2009), in which the assumed spherical olivine particle shrinks from initial diameter of d_0 to $d(t)$ at time t after deposition within the coastal water:

$$d(t) = d_0 - 2\int_0^t R_{\text{diss}}\left(t'\right)\lambda dt' \tag{4}$$

In equation 4, λ, which equals 43.2×10^{-6} m^3 mol^{-1}, is the olivine molar volume and $R_{\text{diss}}(t)$ in unit mol m^{-2} s^{-1} is the dissolution rate at the surface of an olivine particle. $R_{\text{diss}}(t)$ is parameterized as a function of water temperature pH:

$$R_{\text{diss}}(t) = R_0 \cdot f_{\text{pH}}(t) \cdot f_{\text{T}}(t) \tag{5}$$

R_0, which equals 1.58×10^{-10} mol m^{-2} s^{-1}, is the dissolution rate at a temperature of 25°C and pH of 8.2, while $f_{\text{pH}}(t)$ and $f_{\text{T}}(t)$ are dimensionless weighing factors that account for pH and temperature, respectively. f_{pH}, the pH weighing factor, is derived according to the experimental data published by Wogelius and Walther (1991). In their study, the olivine dissolution rate S (mol cm^{-2} s^{-1}) is parameterized as

$$S_* = 9.07\times10^{-12}a_{\text{H}^+}^{0.54} + 5.25\times10^{-15} \tag{6}$$

where a_{H^+} is the hydrogen ion activity in the solution. The particular parameterization we use is based on their 25°C organic-free solution experiments, which are applicable when pH is between 2 and 12.4. Approximating hydrogen ion activity by the hydrogen ion concentration and taking the logarithm relationship between the hydrogen ion concentration and pH, we obtain a pH-weighting factor, f_{pH}, by normalizing equation 6 to its value at a pH value of 8.2. When the ambient pH is below (above) 8.2, the olivine dissolution rate will be enhanced (inhibited) in proportion to this weighing factor:

$$f_{\text{pH}} = \frac{S_*}{S_*(\text{pH}=8.2)} = 1.623\times10^{(3-0.54\times\text{pH})} + 0.9394 \tag{7}$$

For the temperature weighing factor f_{T}, we apply the Arrhenius equation, which parameterizes the olivine reaction rate constant k as a function of absolute seawater temperature T, a pre-exponential constant A, dissolution activation energy E_{a}, and the universal gas constant R:

$$k = Ae^{-E_{\text{a}}/(RT)} \tag{8}$$

We derive the temperature weighing factor f_{T} from two data points in Hangx and Spiers (2009) as the quotient of $k(T)$ for the k-value at a sea temperature of 25°C (298.15 K). We set the activation energy E_{a} to 79.5 kJ mol^{-1} (Hangx & Spiers, 2009) and the universal gas constant to 8.314 J mol^{-1} K^{-1}. Accordingly f_{T} can be written as:

$$f_{\text{T}} = \frac{k(T)}{k(T=298.15)} = e^{3.207-\frac{79.5\times10^3}{83.1451\times T}} \tag{9}$$

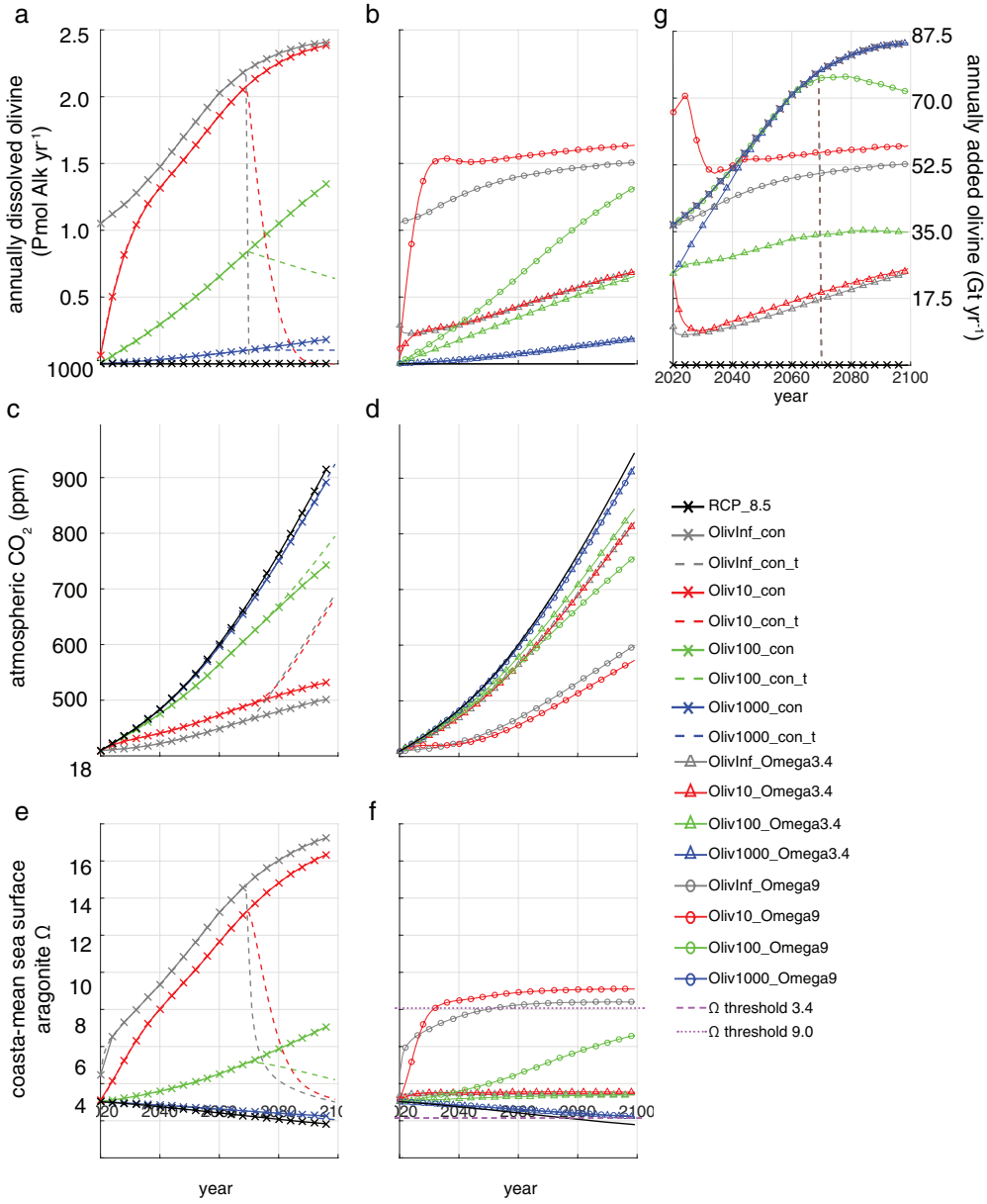

Figure 1. Time series of annual olivine dissolution (a, b), the atmospheric CO_2 concentration (c, d), the coastal-mean sea surface aragonite Ω in COA regions (e f), and annually added olivine (g) in both olivine mass and alkalinity units. For (a)–(f), simulations with continuous olivine supplies are shown in the left column, simulations with local Ω thresholds are shown in the middle column. *RCP_8.5* denotes the RCP 8.5 control run without COA. Please note that the annual olivine addition in the runs with continuous olivine supply is the same for all grain sizes. In the *OlivInf_con run* annually dissolved olivine equals olivine addition (gray curve in panel (a)).

We focus only on the effects of temperature and pH on dissolution because other potentially important factors such as reduced pH in sediments due to the degradation of organic matter, benthic macrofauna sediment bioturbation and ingestion, and wave action (Montserrat et al., 2017) are not resolved in our model.

Since for stoichiometric dissolution 1 mol of olivine is equivalent to adding 4 mol of alkalinity to the seawater, we mathematically simulate olivine dissolution by increasing the surface alkalinity in this ratio in the respective surface ocean model grid cells. We thus quantify and present olivine addition and dissolution in terms of "alkalinity units" (Alk), which is four times the respective molar value of olivine, with only exceptions in Figures 1 and 3 where mass units for olivine addition and dissolution are adopted.

2.3. COA Experimental Design

The model is spun-up for 10,000 years with a prescribed preindustrial atmospheric CO_2 concentration. It is then run for another 200 years without prescribing CO_2, before it is forced with historical CO_2 emissions from 1765 until the year 2005. Thereafter, the RCP (representative concentration pathway) 8.5 high CO_2 emissions scenario (Meinshausen et al., 2011) is imposed until the end of the year 2099. We ignore greenhouse gas forcing other than CO_2 as well as land use changes. This simulation serves as a control run (*RCP_8.5*), and branching point for all COA simulations, which begin in the year 2020 and continue to be forced with the RCP 8.5 emission scenario.

In our idealistic COA setup we simulate a massive deployment scenario by assuming that olivine is added in proportion to anthropogenic CO_2 emissions following the approach of Ilyina et al. (2013) and using a molar ratio of 1 mol of alkalinity (0.25 mol of olivine) added per mole of CO_2 emitted. The COA experiments are divided into three groups. In the first group, olivine is added continuously and homogenously to coastal grid cells (run names have the suffix "*_con*") in order to investigate the upper limits of COA for different grain sizes. The added olivine is assumed to be spherical and can be either infinitesimally small (*OlivInf_con*), 10 μm (*Oliv10_con*), 100 μm (*Oliv100_con*), or 1000 μm (*Oliv1000_con*) in size. Three additional sensitivity runs following the protocol for run *Oliv100_con* are set up to examine the roles of individual environmental factors, that is, temperature and pH that affect the olivine dissolution process. The first run excludes the olivine dissolution dependency on oceanic pH (*Oliv100_con_noph*), the second excludes the effect of oceanic temperature (*Oliv100_con_nosst*), and the third excludes the effects of both pH and temperature (*Oliv100_con_no*) (see Figure S2 in Supporting Information S1). With a similar model setup to the first group, the second group of experiments investigates the longevity of COA effects by terminating COA in year 2070 (run names have the suffix "*_con_t*"; *OlivInf_con_t*, *Oliv10_con_t*, *Oliv100_con_t*, and *Oliv1000_con_t*).

The third group of model runs is the "Ω threshold group". It consists of eight COA simulations and is designed to investigate a COA implementation with local upper limits based on surface aragonite saturation Ω (i.e., Ω thresholds). Ω thresholds are introduced because the COA input from the first group, which proportionally follows the high CO_2 emission scenario, leads to very high Ω levels at the end-of-the-century (Table 1). We therefore decided to investigate to what extent additional constraints on Ω would reduce the potential of COA. Specifically, the simulated olivine addition, which, for different olivine grain sizes, still starts by adding 1 mol of alkalinity (0.25 mol of olivine) per mole of CO_2 emitted, is stopped whenever local Ω thresholds are reached. As illustrative thresholds, we use a conservative Ω threshold of value 3.4 (*OlivInf_Omega3.4*, *Oliv10_Omega3.4*, *Oliv100_Omega3.4*, *Oliv1000_Omega3.4*), with the idea to avoid aragonite oversaturation higher than typical preindustrial levels (Rockström et al., 2009), and a high value of $\Omega = 9$ (*OlivInf_Omega9*, *Oliv10_Omega9*, *Oliv100_Omega9*, *Oliv1000_Omega9*). In the absence of an established Ω threshold to characterize the general physiological tolerance against alkalinity addition, we choose Ω threshold of 9 as an arbitrary threshold at the high end of what could be viewed as a reasonably safe Ω level. Locally, however, olivine addition is only triggered as long as aragonite Ω is below the respective aragonite Ω threshold in that COA grid cell.

3. Results

For the control run (*RCP_8.5*), simulated atmospheric CO_2 reaches 944 ppm at the end of the 21st century (Table 1), which has a large impact on the climate and biogeochemistry (Figure S3). The North Pacific and North Atlantic display the largest SST increases of about 4°C between years 2020 and 2099 (Figures S3a and S3b). Coastal and global mean surface ocean aragonite Ω drop to 1.80 and 1.60 at the end of the 21st century, respectively (Figure 1 and Figure S4). The largest decline in surface-water aragonite Ω by up to 1.65 relative to year 2020 is simulated for the tropical oceans, coastal and open ocean regions alike (Figures S3c and S3d). Relative to year 2020, the largest pH decline, of about 0.45 (Figures S3e and S3f), is observed in the Arctic Ocean, while the global and coastal average surface ocean pH each drop by around 0.3 (Figure S5).

Cumulative results of the COA runs are listed in Table 1. In the first group of simulations cumulative olivine input reaches 150.86 Pmol Alk (i.e., ~5280 Gt olivine; assuming an olivine molar mass of 140 g mol^{-1}) by year 2099. Only the *OlivInf_con* run exhibits complete olivine dissolution, that is, dissolution equals input. For the other three model runs in this group, the amount of annually dissolved olivine becomes smaller as olivine grain size increases (Figure 1a), although the same amount of olivine is added in these runs. The

Table 1.
Experimental Design and Model Results

Model run	Grain size (μm)	Cumulative olivine dissolution (Pmol Alk)[a]	Cumulative olivine input (Pmol Alk)[a]	Coastal aragonite Ω[b]	Atmospheric CO_2 drawdown (GtC)[c]	Atmospheric CO_2 drawdown (ppm)[c]
OlivInf_con	1/∞	150.86	150.86	17.4	−931.8	−438.9
Oliv10_con	10	136.09	150.86	16.5	−868.0	−408.8
Oliv100_con	100	53.37	150.86	7.2	−400.6	−188.7
Oliv100_con_no	100	54.23	150.86	7.4	−405.8	−191.4
Oliv100_con_nosst	100	54.26	150.86	7.3	−405.9	−191.5
Oliv100_con_noph	100	53.33	150.86	7.3	−399.6	−188.5
Oliv1000_con	1000	6.64	150.86	2.2	−53.3	−25.1
OlivInf_con_t	1/∞	80.63	80.63	3.0	−539.3	−254
Oliv10_con_t	10	80.63	80.63	3.2	−554.0	−260.9
Oliv100_con_t	100	41.49	80.63	4.2	−317.8	−149.7
Oliv1000_con_t	1000	5.30	80.63	2.1	−42.5	−20.0
OlivInf_Omega3.4	1/∞	34.45	34.44	3.4	−262.6	−123.7
Oliv10_Omega3.4	10	34.44	38.64	3.5	−264.7	−124.7
Oliv100_Omega3.4	100	27.21	72.35	3.4	−212.9	−100.3
Oliv1000_Omega3.4	1000	6.20	146.02	2.2	−49.9	−23.5
OlivInf_Omega9	1/∞	107.98	107.98	8.4	−732.7	−345.1
Oliv10_Omega9	10	118.52	128.60	9.1	−789.6	−371.9
Oliv100_Omega9	100	52.41	144.03	6.6	−395.0	−186.0
Oliv1000_Omega9	1000	6.64	150.86	2.2	−53.28	−25.1

[a]Integrations are undertaken from year 2020 to year 2099. The olivine molar mass is assumed to be 140 g mol^{-1}. Values from columns "cumulative olivine dissolution" and "cumulative olivine input" are presented in alkalinity units (Pmol Alk).
[b]Annual-mean sea surface aragonite Ω in year 2099 of coastal grid boxes where COA has been implemented. The value in the control run, *RCP_8.5*, is 1.80 (The mean is computed as an area weighted arithmetic mean). For reference the global mean sea surface aragonite Ω for *RCP_8.5* run is 1.60.
[c]Annual-mean atmospheric CO_2 differences relative to the control run *RCP_8.5* in year 2099 (2005 GtC, 944.4 ppm).

ongoing dissolution of accumulated, left-over undissolved olivine from previous additions leads to a more rapid increase in annual olivine dissolution in runs *Oliv10_con* and *Oliv100_con* relative to *OlivInf_con* later in the century (as it does for *Oliv1000_con* when extended over multi-centennial timescales). By the year 2099, the accumulated amounts of dissolved olivine for *Oliv10_con*, *Oliv100_con* and *Oliv1000_con* are 90.2%, 35.3%, and 4.4% (i.e., the dissolution ratio, see Table S1 for details) of the olivine input. Overall, the olivine dissolution ratios from our experiments are close to the analytical solutions given by Hangx and Spiers (2009). As the olivine grain diameter increases from infinitesimal to 1000 μm, the atmospheric CO_2 reduction relative to the control run decreases from 439 to 25 ppm in the year 2099 (Table 1 and Figure 1b) in the chosen high-emission scenario. Very high aragonite Ω levels are reached in these group-one COA implementations by year 2099: Averaged over all coastal grid boxes between 58.5°N and 59.4°S, Ω reaches values well above 16 in runs *OlivInf_con* and *Oliv10_con* (Table 1 and Figure 1c) and locally aragonite Ω reaches values as high as 40. In this group, coastal-mean sea surface pH from *OlivInf_con*, *Oliv10_con* and *Oliv100_con* run increases, but decreases for *Oliv1000_con*. By year 2099, coastal-mean sea surface pH from *OlivInf_con* and *Oliv10_con* runs have reached values higher than 8.6 (Figure S5). Interestingly, not accounting for temperature and pH when calculating olivine dissolution, that is, the *Oliv100_con_no*, *Oliv100_con_nosst*, and *Oliv100_con_noph* simulations, has little impact on the magnitude of atmospheric CO_2 drawdown or coastal-mean aragonite Ω (Table 1).

Several runs from the second group COA-termination runs show a rapid drop in the amount of annually dissolved olivine and in the coastal-mean aragonite Ω and pH levels after year 2070 when compared to

those runs without termination (Figures 1a and 1e). The drop is steeper when the grain size is smaller, while in experiments with larger grain size, undissolved olivine deposited before 2070 buffers this decrease. A related effect of left-over undissolved olivine is the much slower decline in coastal-mean aragonite Ω levels after termination for the runs with larger olivine grain sizes. Therefore, COA-driven atmospheric CO_2 uptake can continue after COA termination, especially for model runs with large olivine grain size. Thus, by the end of the 21st century, almost identical amounts of olivine have dissolved in the *OlivInf_con_t* and *Oliv10_con_t* runs, although atmospheric CO_2 is slightly lower in *Oliv10_con_t* than *OlivInf_con_t* (Table 1). As expected, for all grain sizes atmospheric CO_2 increases faster after termination of COA in year 2070 compared to model runs with continued COA (Figure 1c).

In the "Ω threshold" model runs, atmospheric CO_2 from the *OlivInf_Omega3.4*, *Oliv10_Omega3.4*, *Oliv100_Omega3.4*, *OlivInf_Omega9*, and *Oliv10_Omega9* simulations is reduced by 124, 125, 100, 345, and 371 ppm, respectively, relative to the control run in year 2099 (Table 1 and Figure 1d). However, only some of the simulations end up near their respective coastal-mean aragonite Ω thresholds (Figure 1f). For model runs with larger olivine grain size, that is, the *Oliv1000_Omega3.4*, *Oliv100_Omega9*, and *Oliv1000_Omega9* simulations, where olivine addition is mostly not constrained by the threshold (i.e., additions are similar to that of the first group of experiments; Figure 1 and Table 1), this is because of a relatively low rate of dissolution. Interestingly, in run *OlivInf_Omega9* the coastal-mean aragonite Ω is also always lower than the threshold, while the threshold is obviously crossed in the *Oliv10_Omega9* run (Figure 1f). This is because annually dissolved olivine at the beginning of COA implementation is much lower in the *Oliv10_Omega9* run when compared to the *OlivInf_Omega9* run (Figure 1g). This allows more olivine to be added early in the *Oliv10_Omega9* run, when compared to the *OlivInf_Omega9* run, since the threshold is not reached until at a later time. Such added, but undissolved olivine in the early part of the *Oliv10_Omega9* run, significantly increases alkalinity in the following years as it continues to dissolve, leading to a higher overall coastal-mean aragonite Ω than that of the *OlivInf_Omega9* run (Figures 1f and S7). Because of strong seasonal fluctuations in carbonate chemistry and Ω (see example in Figure S8), there may, in our setup, also be olivine addition during parts of the year, when Ω seasonally drops below the threshold, even though the annual-mean Ω value is well above the threshold.

Exactly how COA perturbs ocean biogeochemistry is strongly affected by the chosen COA implementation scenario. For example, when COA is implemented homogenously in coastal seas in the first group of experiments, olivine dissolution for noninfinitesimally small grain sizes is lower in high latitudes, because lower sea surface temperatures significantly slow down dissolution (Figure S2). We use the results of model run *Oliv100_Omega3.4* to show in more detail how COA affects ocean biogeochemistry and carbon uptake with our CO_2 based addition target and threshold limiting approach. From a global perspective, cumulative olivine dissolution varies spatially among our defined coastal grid boxes (Figure 2a). The biggest COA-induced CO_2 uptake (Figure 2b) occurs along mid- to high latitude coasts. Compared to control run, there is less CO_2 uptake by the ocean and even outgassing from the ocean far from where olivine was added because of the COA-induced decrease in atmospheric CO_2 partial pressure. As a result of accumulated olivine dissolution and ocean circulation, COA-induced ocean storage of CO_2 sequestered from the atmosphere is mainly located in mid- to high-latitudes as well (Figures S9 and S10). Global-mean aragonite Ω and pH both decline by a smaller amount than in the control run (Figures 2c, S4, S5, and S11). Although we stop adding olivine at the aragonite Ω thresholds, many coastal grid boxes (>6% of the entire ocean) end up with an annual-mean aragonite Ω that is higher than 3.4 or 9.0 (Figures 2d and S12). Thus, due to seasonal Ω variability, left-over undissolved olivine from previous additions, and our chosen olivine deployment scheme, annual-mean Ω is not in perfect agreement with the 3.4 or 9.0 thresholds everywhere (Figures S7 and S8).

4. Discussion

In our idealized modeling study, we investigate to what extent the addition of olivine to coastal waters could mitigate the rise of atmospheric CO_2 levels in an assumed 21st century high-emission scenario. Specifically, we examine the potential of a relatively small ocean area to take up CO_2 under different assumptions about olivine grain size and upper limits for a tolerable aragonite saturation state Ω. To this extent, we account only for perceived key factors that could affect olivine dissolution and their effects on carbonate chemistry, but note that other factors such as contamination by trace metals like nickel and iron, the addition of silicate,

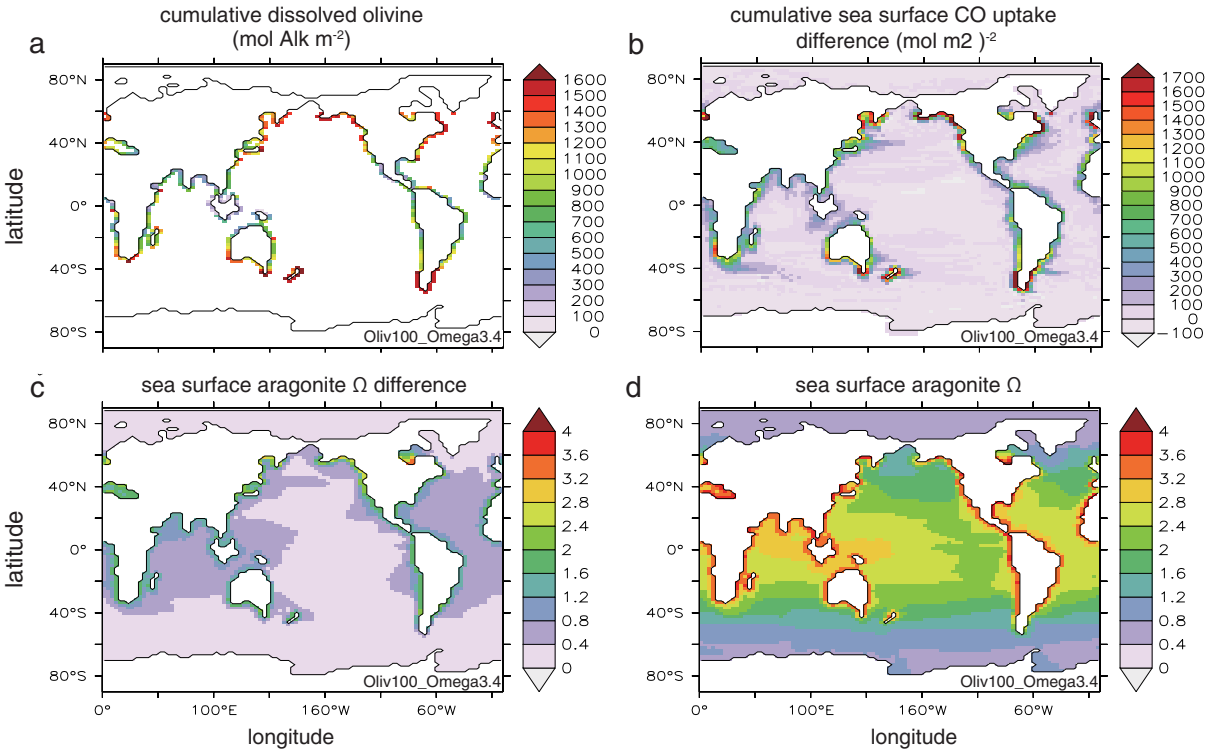

Figure 2. The year 2099 global distribution of cumulative dissolved olivine (a), COA-induced sea surface CO_2 uptake (b), the COA-induced sea surface aragonite Ω difference relative to control run (c) and sea surface aragonite Ω (d), for the *Oliv100_Omega3.4* simulation, where 100 μm olivine grains are added in proportion to RCP 8.5 CO_2 emissions (i.e., 1 mol of alkalinity per mole of emitted CO_2) until a sea surface aragonite Ω threshold of 3.4 is reached.

sediment bioturbation and irrigation by benthic macrofauna, and wave action (Montserrat et al., 2017) may all play an important role in affecting dissolution and the biogeochemical consequences of COA. In experiments where the olivine grain diameter is set to "infinitesimal," we assume that the homogenously and continuously added olivine dissolves instantaneously, independent of ambient pH and temperature. Such highly idealized experiments were designed to provide an upper limit for the CO_2 sequestration potential (Table 1) and might also be used to assess possible effects of adding alkalinity from other easily dissolved sources (e.g., $Ca(OH)_2$).

The model runs with olivine added in proportion to RCP 8.5 CO_2 emissions (i.e., 1 mol of alkalinity per mole of emitted CO_2) indicate that adding this much olivine in an attempt to sequester most of the emissions, would result in very high levels of coastal-mean aragonite Ω that exceed values of 16 (Figure 1e) and have a pH higher than 8.6 (Figure S5) for the simulations with the smallest grain sizes (infinitesimal and 10 μm). Under such high alkalinity and pH levels, spontaneous, abiotic calcium carbonate (Morse et al., 2003) as well as calcium phosphate precipitation (Song et al., 2002) will likely occur (equations 10 and 11), which would increase sea surface pCO_2 (Pilson, 2013) and thereby counteract the intended increase of CO_2—uptake (equation 10):

$$Ca^{2+} + 2HCO_3^- \rightarrow CaCO_3 + CO_2 + H_2O \quad (10)$$

$$3Ca^{2+} + 2PO_4^{3-} \rightarrow Ca_3\left(PO_4\right)_2 \quad (11)$$

The increase of Ω, pH, and the carbonate ion concentration beyond current or preindustrial levels may also have unforeseen and potentially detrimental biological impacts (Renforth & Henderson, 2017). For example, $Ca(OH)_2$ addition was found to disrupt the acid-base balance in *Carcinus maenas*, resulting in slight respiratory alkalosis and hyperkalemia (Cripps et al., 2013). Reduced carbon and nitrogen fixation rates have also been demonstrated in the cyanobacterium *Trichodesmium* at low pCO_2 (Barcelos e Ramos et al., 2007). For larger grain sizes, the slower dissolution slows down the increase in Ω, pH, and the carbonate ion

Table 2.
Grinding Process Corrected CO_2 Sequestration Potential

Model run	COA efficiency (%)[a]	Olivine dissolution ratio (%)	Grinding offset (%)[b]	Ocean carbon sequestration (GtC)[c]		Actual offset ratio (%)
				P_0	P	$(P_0 - P)/P_0$
OlivInf_con	60.33	100	–	1092	–	–
Oliv10_con	61.57	90.21	17.4	1005	811	19.3
Oliv100_con	68.82	35.34	1.34	441	424	3.80
Oliv1000_con	72.24	4.40	0.49	58	51	12.1
OlivInf_con_t	64.61	100	–	625	–	–
Oliv10_con_t	65.94	100	17.4	638	527	17.4
Oliv100_con_t	70.06	51.46	1.34	349	340	2.60
Oliv1000_con_t	72.24	6.57	0.49	46	43	6.50
OlivInf_Omega3.4	69.70	100	–	288	–	–
Oliv10_Omega3.4	70.27	89.15	17.4	290	234	19.3
Oliv100_Omega3.4	71.09	37.61	1.34	232	224	3.40
Oliv1000_Omega3.4	72.75	4.24	0.49	54	48	11.1
OlivInf_Omega9	64.99	100	–	842	–	–
Oliv10_Omega9	64.22	92.15	17.4	913	741	18.8
Oliv100_Omega9	69.07	36.38	1.34	434	418	3.70
Oliv1000_Omega9	72.24	4.40	0.49	58	51	12.1

[a]"COA efficiency" is defined as the amount of sequestrated CO_2 for one unit added alkalinity.
[b]Values are from Hangx and Spiers (2009). Total emission column for grain size 10, 100, and 1000 μm, referring to the ratio of emitted CO_2 during the grinding process versus total CO_2 sequestration.
[c]Values are given as carbon stocks change by year 2099. P_0 is the one derived from model output directly as cumulative COA carbon uptake, P is the same to P_0 considering grinding offset. P_0 is calculated following equation: $P_0 = M_c \cdot V_c \cdot (R_{diss} \cdot R_{DIC/TA} - R_{DIC/TA} \cdot R_g)$, where V_c is the cumulative olivine input by the year 2099 and R_{diss} is the cumulative dissolution ratio for olivine. $R_{DIC/TA}$ is "COA efficiency." R_g is the grinding offset (as a percentage) when grinding related CO_2 emissions are included (Hangx & Spiers, 2009), and M_c is the carbon molar mass 12 g mol^{-1}.

concentration (as well as the sequestration of CO_2), while undissolved olivine grains may have undesired side effects on benthic ecosystems via mechanical and optical stress.

The simulations where COA is discontinued after year 2070 (i.e., the "*_con_t*" runs) show that should COA abruptly cease, for whatever reason, the olivine that was added, but that did not dissolve before COA stops, will continue to dissolve thereafter and enhance ocean alkalinity. These results suggest that if our COA termination simulations were continued for long enough, the added olivine in all experiments would completely dissolve. However, as the olivine grain size in the experiments increases, the time required for complete dissolution also increases. Although, in cases where the grain size is large and dissolution is slow, it is possible that in the real world some olivine may be permanently buried in sediments and never dissolve. The time lag between olivine addition and its ultimate effect on ocean chemistry and atmospheric CO_2 needs to be taken into account when planning to stop COA because a climate or environmental target has been met or because side effect impacts need to be stopped.

Having identified unreasonably high values of the aragonite saturation level Ω in the first group of simulations, where olivine was added in amounts proportional to anthropogenic CO_2 emissions, simulations of the third group employ an upper limit of Ω, at which the addition of olivine is stopped. This imposed limitation reduces the potential of COA as a "stand-alone" CDR method during a business-as-usual emission scenario (Figure 3). In the *Oliv10_Omega3.4* simulation that has the highest CO_2 sequestration potential among the aragonite Ω threshold 3.4 runs, about 264 GtC (125 ppm) can be sequestered from the atmosphere by COA by the end-of-the-century if the olivine supply is stopped whenever Ω exceeds 3.4. The amount of carbon sequestered increases to 790 GtC (372 ppm) if olivine addition is stopped only at a higher Ω level of 9. With

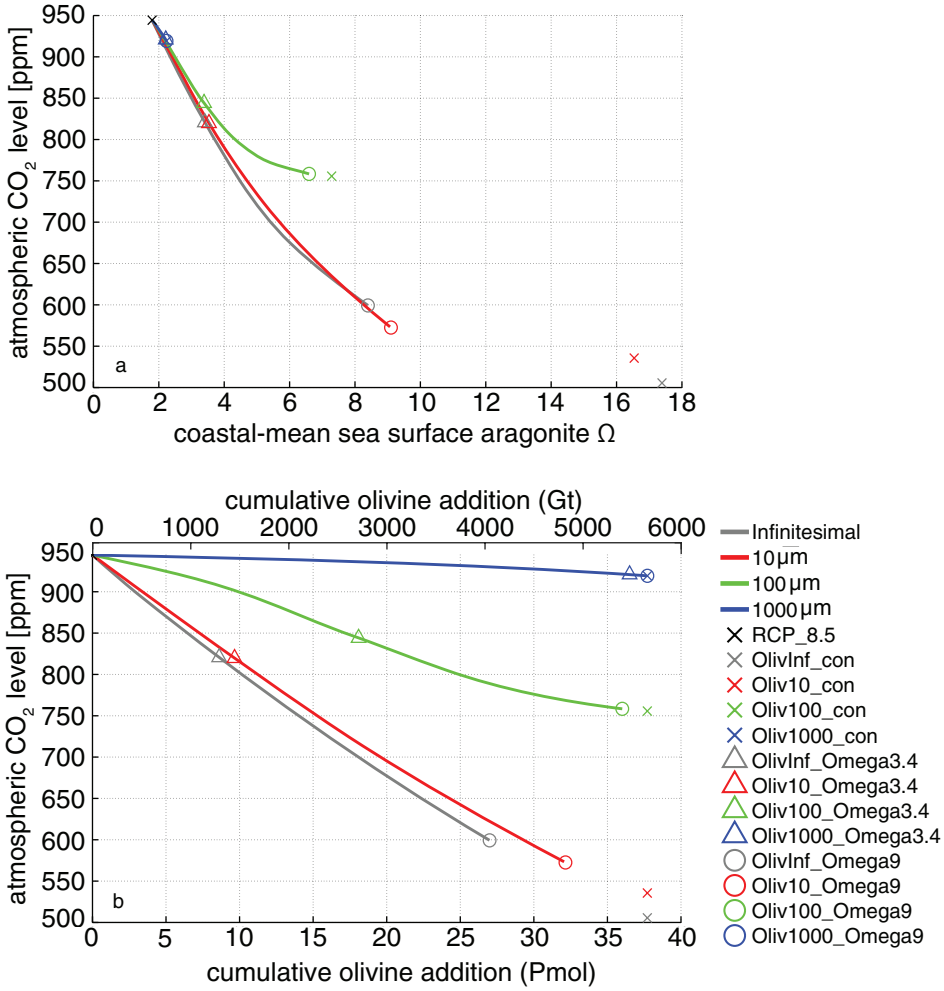

Figure 3. Experiment relationships between simulated atmospheric CO_2 and coastal-mean aragonite Ω in COA implemented regions in the year 2099 (a), and between atmospheric CO_2 and cumulative olivine input (b; molar units on bottom *x*-axis with mass units on top *x*-axis).

our experimental setup, 10 µm olivine grains have an even higher CO_2 sequestration potential than the "infinitesimally" small olivine grains, a result that can be explained by the ongoing dissolution of olivine grains already in the water, but that are undissolved at the time the Ω threshold is reached and olivine addition is stopped (Figures 3 and S7). For the scenario of run *Oliv10_Omega3.4* about 1352 Gt olivine would need to be mined, processed, and added to coastal seas until the end-of-the-century. For *Oliv10_Omega9* more than 4501 Gt olivine would have to be dissolved. These olivine supply rates are on average equivalent to annual rates of about 16.5–56 Gt yr^{-1} and significantly exceed current global mining production of olivine (~70 Mt yr^{-1}; Bide et al., 2014; Fortey, 2000). They compare in scale with the current global mining of coal (~8 Gt yr^{-1}; International Energy Agency, 2014) and construction materials (e.g., sand, gravel, and stone, ~47–59 Gt yr^{-1}; Krausmann et al., 2008). The feasibility of mining such quantities of olivine needs to be assessed, which, however, is beyond the scope of this study.

CO_2 emissions associated with COA preparation and operation processes, that is, mining, grinding and transport are neglected in these experiments. The recent Paris Climate Agreement sets the aspirational goal of limiting global warming to less than 2°C, and preferably to 1.5°C, to significantly reduce risks and impacts of climate change (United Nations Framework Convention on Climate Change [UNFCCC], 2015). To reach the 2°C target, atmospheric CO_2 levels of a business-as-usual emission scenario would have to be reduced by approximately 1000 GtC by the end of this century (Gasser et al., 2015). According to our results (Table 1), COA alone, as shown by, for example, the *Oliv10_con* run could not achieve such a drawdown (Figure S13),

even if massive amounts of olivine were added to the point where seawater carbonate chemistry is substantially perturbed. However, such a massive deployment might not be needed in limited-warming socioeconomic scenarios that already include CDR (other than COA) and also assume decreasing CO_2 emissions (Chen & Tavoni, 2013; Kriegler et al., 2016; Riahi et al., 2017). In these lower emission scenarios our results imply that COA may have the potential to be a viable CDR strategy that could help to meet the 2°C or 1.5°C targets if emission reductions alone are not enough. However, more research is needed to better understand the economics, potential, and risks of COA in such scenarios as our highly idealized simulations were designed to investigate upper limits of COA and not to help meet specific temperature targets.

The above analysis is based on idealized simulations where COA associated CO_2-costs of mining, grinding, and transport processes are not considered to offset COA carbon sequestration. To gain any significant mitigation effect through COA, olivine mining would have to be expanded by more than two orders of magnitude, and likely other alkaline minerals (e.g., lime) would have to be considered for COA usage as well. Though CO_2 emissions from mining and transport are minor (Hangx & Spiers, 2009; Moosdorf et al., 2014), grinding olivine minerals into small particles is energy intensive and can significantly offset the CDR potential of COA if fossil fuels are combusted to power the grinding (Table 2). For example, Hangx and Spiers (2009) estimated that grinding bulk olivine rock into grains that are smaller than 10 μm with fossil fuel powered machinery would offset at least 17% of the CO_2 sequestered by COA. Hence, in the following analysis we evaluate the CO_2 sequestration offset due to grinding for model runs with grain sizes equal to or larger than 10 μm (Table S1). Note that carbon sequestered in the ocean is not equivalent to atmospheric CO_2 drawdown due to carbon cycle feedbacks, that is, backfluxes, from the terrestrial carbon pool. In general, around 17.4%–19.3% of the sequestrated CO_2 would have to be offset for the 10 μm runs if grinding is powered by fossil fuels. For 100 and 1000 μm runs the offsets are 2.6%–3.8% and 6.5%–12.1%, respectively. When compared to the 100 μm run, the larger offset in the 1000 μm run, which occurs despite lower energy costs per ton of ground olivine, is due to the much lower dissolution and thus, lower CO_2 sequestration during the time period considered. Overall, our results indicate that on an end-of-the-century time scale smaller olivine grains (10–100 μm) have advantages in terms of COA-induced CO_2 removal, even when the energy requirements of grinding are accounted for.

Observational evidence and model projections have indicated that coastal regions are among the areas most vulnerable to global change, especially in regards to eutrophication and acidification (Doney, 2010; Feely et al., 2008; Kroeze et al., 2013). In the tropical oceans, coral ecosystems are threatened by ocean acidification and warming (Hoegh-Guldberg et al., 2007). If COA would be applied at the scale illustrated in this study and olivine was ground to allow for rapid dissolution, our results suggest that COA may have the potential to protect coastal regions from acidification (Table 1, Figures 1c,d, 2c,d, 3a and S5). However, there are also potential side effects to be considered. The addition of olivine, which contains iron and silicon, may act as a fertilizer and could cause or increase coastal ecological structural shifts (Blain et al., 2007; Hauck et al., 2016). Considering silicon input alone, adding olivine can easily lead to an artificial silicon influx of up to 0.43 kg m^{-2} yr^{-1}, whereas the global silicon flux is estimated 6.2 teramoles per year (~0.48 kg m^{-2} yr^{-1} on average) (Bernard et al., 2011). Particulate olivine grains also have specific optical properties related to the green color of the crystals. Adding olivine to seawater (or beaches) could thus change the water transparency, underwater light spectrum, and sea surface albedo. Optical perturbations may also arise from spontaneous calcium carbonate precipitation (Broecker & Takahashi, 1966), which might be triggered by a COA-induced increase in calcium carbonate saturation levels and possible changes in the magnesium to calcium ratio (Mekmene et al., 2009; Reddy & Wang, 1980).

5. Conclusions

For the first time, olivine-based COA is simulated in a fully coupled global Earth system model with an explicit parameterization of the olivine dissolution process. We evaluated the CDR potential of COA for differently sized grains of olivine, as well as the resulting ocean carbonate chemistry perturbations during a business-as-usual high CO_2 emission scenario. Our simulation experiments investigate both chemically unconstrained massive olivine additions and chemically constrained Ω-threshold approaches from year 2020 to 2099. Overall, simulations assuming smaller olivine grains demonstrated higher efficiencies than those with larger grains.

If current olivine production can be enhanced by more than two orders of magnitude, if side effects are deemed acceptable, and if society is willing to pay to remove CO_2 from the atmosphere, olivine-based COA may have a considerable CDR potential. Furthermore, it could help to mitigate coastal ocean acidification and may help to protect tropical coral reefs and other coastal ecosystems from the threat of ocean acidification. More refined regional follow-on studies would be required to assess the technological and environmental feasibility of specific deployment scenarios.

However, our results suggest that at some scale of deployment the side effects of COA, in particular because of altered ocean chemistry, will become substantial and may outweigh the climate mitigation benefits. Determining when the negatives aspects of COA outweigh the positive ones requires further study. Process uncertainties such as the complex factors affecting olivine dissolution, as well as possible side effects due to supply of silica, iron and likely contaminations by heavy metals (Hartmann et al., 2013) should be assessed in the future through both high-resolution modeling and dedicated lab and possibly small-scale in situ experiments. For example, the olivine in this study is assumed to contain no iron (i.e., forsterite — Mg_2SiO_4). However, iron-containing olivine is more naturally abundant (De Hoog et al., 2010), which has implications for COA if such material were used as the presence of iron can influence dissolution. Recent batch reaction experiments in bottles (Montserrat et al., 2017) discovered that a fraction of the olivine-derived alkalinity is consumed by aerobic iron oxidation during the dissolution process. As a result of such process, the alkalinity-induced CO_2 uptake from the atmosphere may be reduced (Griffioen, 2017). These dynamics are not included in our idealized COA experiments and may need further study. Future studies will also need to investigate the implications of different COA deployment strategies, which may be quite different from the homogenous and continuous additions in some of our simulations, that is, in real-word applications logistical and technical constraints would likely result in spatially and temporally heterogeneous COA.

Acknowledgments
This is a contribution to the SPP 1689 "Climate Engineering — risks, challenges, opportunities?" funded by the Deutsche Forschungsgemeinschaft (DFG). E. Y. Feng's research project is also supported by the Cluster of Excellence 'The Future Ocean' (CP1780). "The Future Ocean" is funded within the framework of the Excellence Initiative by the Deutsche Forschungsgemeinschaft (DFG) on the behalf of the German federal and state governments. Additional funding is provided by the BMBF BIOACID Program (FKZ 03F0728A) to W.K. All authors declare that they have no potential conflicts of interests. Model outputs and other data to produce figures/tables is available from http://data.geomar.de/thredds/catalog/open_access/feng_et_al_2017_ef/catalog.html.

References

Albright, R., Caldeira, L., Hosfelt, J., Kwiatkowski, L., Maclaren, J. K., Mason, B. M., … Caldeira, K. (2016). Reversal of ocean acidification enhances net coral reef calcification. *Nature*, *531*, 362–365. https://doi.org/10.1038/nature17155

Barcelos e Ramos, J., Biswas, H., Schulz, K. G., LaRoche, J., & Riebesell, U. (2007). Effect of rising atmospheric carbon dioxide on the marine nitrogen fixer Trichodesmium. *Global Biogeochemical Cycles*, *21*, GB2028.

Bellamy, R., Chilvers, J., Vaughan, N. E., & Lenton, T. M. (2012). A review of climate geoengineering appraisals. *WIREs Climate Change*, *3*, 597–615. https://doi.org/10.1002/wcc.197

Bernard, C. Y., Dürr, H. H., Heize, C., Segschneider, J., & Maier-Reimer, E. (2011). Contribution of riverine nutrients to the silicon biogeochemistry of the global ocean — A model study. *Biogeosciences*, *8*, 511–564.

Bide, T. P., Styles, M. T., & Naden, J. (2014). An assessment of global resources of rocks as suitable raw minerals for carbon capture and storage by mineralization. *Applied Earth Science*, *123*, 179–195. https://doi.org/10.1179/1743275814Y.0000000057

Bitz, C. M., & Liscomb, W. H. (1999). An energy-conserving thermodynamic model of sea ice. *Journal of Geophysical Research*, *104*, 15669–15677. https://doi.org/10.1029/1999JC900100

Blain, S., Quéguiner, B., Armand, L., Belviso, S., Bombled, B., Bopp, L., … Wagener, T. (2007). Effect of natural iron fertilization on carbon sequestration in the Southern Ocean. *Nature*, *446*, 1070–1074. https://doi.org/10.1038/nature05700

Broecker, W. S., & Takahashi, T. (1966). Calcium carbonate precipitation on the Bahama banks. *Journal of Geophysical Research*, *71*, 1575–1602. https://doi.org/10.1029/JZ071i006p01575

Chen, C., & Tavoni, M. (2013). Direct air capture of CO_2 and climate stabilization: A model based assessment. *Climatic Change*, *118*, 59–72. https://doi.org/10.1007/s10584-013-0714-7

Cripps, G., Widdicombe, S., Spicer, J. I., & Findlay, H. S. (2013). Biological impacts of enhanced alkalinity in *Carcinus maenas*. *Marine Pollution Bulletin*, *71*, 190–198. https://doi.org/10.1016/j.marpolbul.2013.03.015

De Hoog, J. C. M., Gall, L., & Cornell, D. H. (2010). Trace-element geochemistry of mantle olivine and application to mantle petrogenesis and geothermobarometry. *Chemical Geology*, *270*, 196–215. https://doi.org/10.1016/j.chemgeo.2009.11.017

De Rooij, J. F., Heughebaert, J. C., & Nancollas, G. H. (1984). A pH study of calcium phosphate seeded precipitation. *Journal of Colloid and Interface Science*, *100*, 350–358. https://doi.org/10.1016/0021-9797(84)90440-5

Doney, S. C. (2010). The growing human footprint on coastal and open-ocean biogeochemistry. *Science*, *328*, 1512–1516. https://doi.org/10.1126/science.1185198

Eby, M., Weaver, A. J., Alexander, K., Zickfeld, K., Abe-Ouchi, A., Cimatoribus, A. A., … Zhao, F. (2013). Historical and idealized climate model experiments: An intercomparison of Earth system models of intermediate complexity. *Climate of the Past*, *9*, 1111–1140. https://doi.org/10.5194/cp-9-1111-2013

Fanning, A. F., & Weaver, A. J. (1996). An atmospheric energy-moisture balance model: Climatology, interpentadal climate change, and coupling to an ocean general circulation model. *Journal of Geophysical Research*, *101*, 15111–15128. https://doi.org/10.1029/96JD01017

Feely, R. A., Sabine, C. L., Hernandez-Ayon, J. M., Ianson, D., & Hales, B. (2008). Evidence for upwelling of corrosive "acidified" water onto the continental shelf. *Science*, *320*, 1490–1492. https://doi.org/10.1126/science.1155676

Feng, E. Y., Keller, D. P., Koeve, W., & Oschlies, A. (2016). Could artificial ocean alkalinization protect tropical coral ecosystems from ocean acidification? *Environmental Research Letters*, *11*, 074008. https://doi.org/10.1088/1748-9326/11/7/074008

Fortey, N. J. (2000). In D. J. Vaughan & R. A. Wogelius (Eds.), *Environmental Mineralogy*. Budapest: Eötvös University Press.

Gasser, T., Guivarch, C., Tachiiri, K., Jones, C. D., & Ciais, P. (2015). Negative emission physically needed to keep global warming below 2 °C. *Nature Communications*, *6*, 7958. https://doi.org/10.1038/ncomms8958

González, M. F., & Ilyina, T. (2016). Impacts of artificial ocean alkalinization on the carbon cycle and climate in Earth system simulations. *Geophysical Research Letters*, *43*, 6493–6502. https://doi.org/10.1002/2016GL068576

Griffioen, J. (2017). Enhanced weathering of olivine in seawater: The efficiency as revealed by thermodynamic scenario analysis. *Science of the Total Environment*, *575*, 536–544. https://doi.org/10.1016/j.scitotenv.2016.09.008

Hangx, S. J. T., & Spiers, J. C. (2009). Coastal spreading of olivine to control atmospheric CO_2 concentrations: A critical analysis of viability. *International Journal of Greenhouse Gas Control*, *3*, 757–767. https://doi.org/10.1016/j.ijggc.2009.07.001

Hartmann, J., West, A. J., Renforth, P., Köhler, P., Rocha, C. L. D. L., Wolf-gladrow, D. A., Dürr, H. H., & Scheffran, J. (2013). Enhanced chemical weathering as a geoengineering strategy to reduce atmospheric carbon dioxide, supply nutrients, and mitigate ocean acidification. *Reviews of Geophysics*, *51*, 113–149. https://doi.org/10.1002/rog.20004

Harvey, L. D. D. (2008). Mitigating the atmospheric CO_2 increase and ocean acidification by adding limestone powder to upwelling regions. *Journal of Geophysical Research*, *113*, 2156–2202.

Hauck, J., Köhler, P., Wolf-Gladrow, D. A., & Völker, C. (2016). Iron fertilisation and century-scale effects of open ocean dissolution of olivine in a simulated CO_2 removal experiment. *Environmental Research Letters*, *11*, 024007. https://doi.org/10.1088/1748-9326/11/2/024007

Hoegh-Guldberg, O., Mumby, P. J., Hooten, A. J., Steneck, R. S., Greenfield, P., Gomez, E., … Hatziolos, M. E. (2007). Coral reefs under rapid climate change and ocean acidification. *Science*, *318*, 1737–1742. https://doi.org/10.1126/science.1152509

House, K. Z., House, C. H., Schrag, D. P., & Aziz, M. J. (2007). Electrochemical acceleration of chemical weathering as an energetically feasible approach to mitigating anthropogenic climate change. *Environmental Science & Technology*, *41*, 8464–8470. https://doi.org/10.1021/es0701816

Ilyina, T., Wolf-Gladrow, D., Munhoven, G., & Heinze, C. (2013). Assessing the potential of calcium-based artificial ocean alkalinization to mitigate rising atmospheric CO_2 and ocean acidification. *Geophysical Research Letters*, *40*, 5909–5914. https://doi.org/10.1002/2013GL057981

International Energy Agency (2014). *World Energy Outlook*, Paris. Retrieved from www.worldenergyoutlook.org

IPCC Core Writing Team (2014). Climate change 2014: Synthesis report. In *Contribution of Working Groups I, II and III to the Fifth Assessment Report of the Intergovernmental Panel on Climate Change*. Geneva, Switzerland: IPCC.

Keller, D. P., Oschlies, A., & Eby, M. (2012). A new marine ecosystem model for the University of Victoria Earth System climate model. *Geoscientific Model Development*, *5*, 1195–1220. https://doi.org/10.5194/gmd-5-1195-2012

Keller, D. P., Feng, E. Y., & Oschlies, A. (2014). Potential climate engineering effectiveness and side effects during a high carbon dioxide-emission scenario. *Nature Communications*, *5*, 3304. https://doi.org/10.1038/ncomms4304

Kheshgi, H. S. (1995). Sequestering atmospheric carbon dioxide by increasing ocean alkalinity. *Energy*, *20*, 915–922. https://doi.org/10.1016/0360-5442(95)00035-F

Köhler, P., Hartmann, J., & Wolf-Gladrow, D. A. (2010). Geoengineering potential of artificially enhanced silicate weathering of olivine. *Proceedings of the National Academy of Sciences of the United States of America*, *107*, 20228–20233. https://doi.org/10.1073/pnas.1000545107

Köhler, P., Abrams, J. F., Völker, C., Hauck, J., & Wolf-Gladrow, D. A. (2013). Geoengineering impact of open ocean dissolution of olivine on atmospheric CO_2, surface ocean pH and marine biology. *Environmental Research Letters*, *8*, 014009. https://doi.org/10.1088/1748-9326/8/1/014009

Krausmann, F., Fischer-Kowalski, M., Schandl, H., & Eisenmenger, N. (2008). The global sociometabolic transition. *Journal of Industrial Ecology*, *12*, 637–656. https://doi.org/10.1111/j.1530-9290.2008.00065.x

Kriegler, E., Bauer, N., Popp, A., Humpenoeder, F., Leimbach, M., Strefler, J., Baumstark, L., Bodirsky, B. L., Hilaire, J., & Klein, D. (2016). Fossil-fueled development (SSP5): An energy and resource intensive scenario for the 21st century. *Global Environmental Change*, *42*, 297–315.

Kroeze, C., Hofstra, N., Ivens, W., Löhr, A., Strokal, M., & van Wijnen, J. (2013). The links between global carbon, water and nutrient cycles in an urbanizing world—The case of coastal eutrophication. *Current Opinion in Environment Sustainability*, *5*, 566–572. https://doi.org/10.1016/j.cosust.2013.11.004

Kump, L. R., Brantley, S. L., & Arthur, M. A. (2000). Chemical weathering, atmospheric CO_2, and climate. *Annual Review of Earth and Planetary Sciences*, *28*, 611–667. https://doi.org/10.1146/annurev.earth.28.1.611

Landschützer, P., Gruber, N., Bakker, D. C. E., & Schuster, U. (2014). Recent variability of the global ocean carbon sink. *Global Biogeochemical Cycles*, *28*, 927–949. https://doi.org/10.1002/2014GB004853

Locarnini, R. A., Mishonov, A. V., Antonov, J. I., Boyer, T. P., Garcia, H. E., Baranova, O. K., … Seidov, D. (2013). *NOAA Atlas NESDIS 62 World Ocean Atlas 2013 Volume 1: Temperature*.

Maher, K., Johnson, N. C., Jackson, A., Lammers, L. N., Torchinsky, A. B., Weaver, K. L., Bird, D. K., & Brown Jr., G. E. (2016). A spatially resolved surface kinetic model for forsterite dissolution. *Geochimica et Cosmochimica Acta*, *174*, 313–334. https://doi.org/10.1016/j.gca.2015.11.019

Marion, G. M., Millero, F. J., & Feistel, R. (2009). Precipitation of solid phase calcium carbonates and their effect on application of seawater S-A-T-P models. *Ocean Science*, *5*, 285–291. https://doi.org/10.5194/os-5-285-2009

Meinshausen, M., Smith, S. J., Calvin, K., Daniel, J. S., Kainuma, M. L. T., Lamarque, J.-F., … van Vuuren, D. P. P. (2011). The RCP greenhouse gas concentrations and their extensions from 1765 to 2300. *Climatic Change*, *109*, 213–241. https://doi.org/10.1007/s10584-011-0156-z

Meissner, K. J., Weaver, A. J., Matthews, H. D., & Cox, P. M. (2003). The role of land surface dynamics in glacial inception: A study with the UVic earth system model. *Climate Dynamics*, *21*, 515–537. https://doi.org/10.1007/s00382-003-0352-2

Mekmene, O., Quillard, S., Rouillon, T., Bouler, J.-M., Piot, M., & Gaucheron, F. (2009). Effects of pH and Ca/P molar ratio on the quantity and crystalline structure of calcium phosphates obtained from aqueous solutions. *Dairy Science & Technology*, *89*, 301–316. https://doi.org/10.1051/dst/2009019

Meysman, F. G., & Montserrat, F. (2017). Negative CO_2 emissions via enhanced silicate weathering in coastal environments. *Biology Letters*, *13*(4), 20160905. https://doi.org/10.1098/rsbl.2016.0905

Millero, J. F. (2007). The marine inorganic carbon cycle. *Chemical Reviews*, *107*, 308–341. https://doi.org/10.1021/cr0503557

Montserrat, M., Renforth, P., Hartmann, J., Leermakers, M., Knop, P., & Meysman, F. J. R. (2017). Olivine dissolution in seawater: Implications for CO_2 sequestration through enhanced weathering in coastal environments. *Environmental Science & Technology*, *51*, 3960–3972. https://doi.org/10.1021/acs.est.6b05942

Moosdorf, N., Renforth, P., & Hartmann, J. (2014). Carbon dioxide efficiency of terrestrial enhanced weathering. *Environmental Science & Technology*, *48*, 4809–4816. https://doi.org/10.1021/es4052022

Morse, J. M., Gledhill, D. K., and Millero, F. J. (2003). $CaCO_3$ precipitation kinetics in waters from the Great Bahama Bank: Implications for the relationship between bank hydrochemistry and whitings. *Geochimica et Cosmochimica Acta*, *67*(15), 2819–2826. https://doi.org/10.1016/S0016-7037(03)00103-0

National Research Council (2015). *Climate Intervention: Carbon Dioxide Removal and Reliable Sequestration*. Washington, DC: The National Academies Press.

Orr, J. C., Najjar, R., Sabine, C. L., & Joos, F. (1999). *Abiotic-HOWTO. Internal OCMIP Report*. Gif-sur-Yvette, France: LSCE/CEA Saclay.

Pacanowski, R. C. (1996). *MOM2: Documentation, user's guide and reference manual GFDL ocean* (Tech. Rep. 3.2) (329 pp).

Pilson, M. E. Q. (2013). *An Introduction to the Chemistry of the Sea*. Cambridge: Cambridge University Press.

Pokrovsky, O. S., & Schott, J. (2000). Kinetics and mechanism of forsterite dissolution at 25°C and pH from 1 to 12. *Geochimica et Cosmochimica Acta*, *64*, 3313–3325. https://doi.org/10.1016/S0016-7037(00)00434-8

Rau, G. H. (2008). Electrochemical splitting of calcium carbonate to increase solution alkalinity: Implications for mitigation of carbon dioxide and ocean acidity. *Environmental Science & Technology*, *42*, 8935–8940. https://doi.org/10.1021/es800366q

Rau, G. H., & Caldeira, K. (1999). Enhanced carbonate dissolution: A means of sequestering waste CO_2 as ocean bicarbonate. *Energy Conversion and Management*, *40*, 1803–1813. https://doi.org/10.1016/S0196-8904(99)00071-0

Rau, G. H., Caldeira, K., Knauss, K. G., Downs, B., & Sarv, H. (2001). Enhanced carbonate dissolution as a means of capturing and sequestering carbon dioxide. In *First National Conference on Carbon Sequestration* (Vol. *2*, pp. 1–7).

Reddy, M. M., & Wang, K. K. (1980). Crystallization of calcium carbonate in the presence of metal ions: I. Inhabitation by magnesium ion at pH 8.8 and 25°C. *Journal of Crystal Growth*, *50*, 470–480. https://doi.org/10.1016/0022-0248(80)90095-0

Renforth, P., Jenkins, B. G., & Kruger, T. (2013). Engineering challenges of ocean liming. *Energy*, *60*, 442–452. https://doi.org/10.1016/j.energy.2013.08.006

Renforth, P., & Henderson, G. (2017). Assessing ocean alkalinity for carbon sequestration. *Reviews of Geophysics*, *55*, 636–674. https://doi.org/10.1002/2016RG000533

Riahi, K., van Vuuren, D. P., Kriegler, E., Edmonds, J., O'Neill, B. C., Fujimori, S., … Tavoni, M. (2017). The shared socioeconomic pathways and their energy, land use, and greenhouse gas emissions implications: An overview. *Global Environmental Change*, *42*, 153–168. https://doi.org/10.1016/j.gloenvcha.2016.05.009

Rockström, J., Steffen, W., Noone, K., Persson, Å., Chapin, F. S., Lambin, E. F., … Foley, J. A. (2009). A safe operating space for humanity. *Nature*, *461*(24), 472–475. https://doi.org/10.1038/461472a

Schuiling, R. D., & Krijgsman, P. (2006). Enhanced weathering: An effective and cheap tool to sequester CO_2. *Climatic Change*, *74*, 349–354. https://doi.org/10.1007/s10584-005-3485-y

Song, Y., Hahn, H. H., & Hoffmann, E. (2002). The effect of carbonate on the precipitation of calcium phosphate. *Environmental Technology*, *23*, 207–215. https://doi.org/10.1080/09593332508618427

Taylor, L. L., Quirk, J., Thorley, R. M. S., Kharecha, P. A., Hansen, J., Ridgwell, A., Lomas, M. R., Bonwart, S. A., & Beerling, D. J. (2015). Enhanced weathering strategies for stabilizing climate and averting ocean acidification. *Nature Climate Change*, *6*, 402–406. https://doi.org/10.1038/nclimate2882

United Nations Framework Convention on Climate Change (2015). *Adoption of the Paries Agreement* (Rep. No. FCCC/CP/2015/L.9/Rev.1).

Wang, C., Zhang, L., Lee, S., Wu, L., & Mechoso, C. R. (2014). A global perspective on CMIP5 climate model biases. *Nature Climate Change*, *4*, 201–205. https://doi.org/10.1038/nclimate2118

Weaver, A. J., Eby, M., Wiebe, E. C., Bitz, C. M., Duffy, P. B., Ewen, T. L., … Yoshimori, M. (2001). The UVic earth system climate model: Model description, climatology, and applications to past, present and future climates. *Atmosphere-Ocean*, *39*, 361–428. https://doi.org/10.1080/07055900.2001.9649686

Wogelius, R. A., & Walther, J. V. (1991). Olivine dissolution at 25°C: Effects of pH, CO_2, and organic acids. *Geochimica et Cosmochimica Acta*, *55*, 943–954. https://doi.org/10.1016/0016-7037(91)90153-V